

## Experimental study on standard and innovative bolted end-plate beam-to-beam joints under bending

Levente Katula\* and László Dunai

*Department of Structural Engineering, Budapest University of Technology and Economics,  
Műegyetem rkp. 3, H-1111 Budapest, Hungary*

*(Received July 16, 2012, Revised November 20, 2014, Accepted December 01, 2014)*

**Abstract.** The paper presents the details and results of an experimental study on bolted end-plate joints of industrial type steel building frames. The investigated joints are commonly used in Lindab-Astron industrial buildings and are optimized for manufacturing, erection and durability. The aim of the research was to provide an experimental background for the design model development by studying load-bearing capacity of joints, bolt force distribution, and end-plate deformations. Because of the special joint details, (i.e., joints with four bolts in one bolt-row and HammerHead arrangements), the Eurocode 3 standardized component model had to be improved and extended. The experimental programme included six different end-plate and bolt arrangements and covered sixteen specimens. The steel grade of test specimens was S355, the bolt diameter M20, whereas the bolt grade was 8.8 and 10.9 for the two series. The end-plate thickness varied between 12 mm and 24 mm. The specimens were investigated under pure bending conditions using a four-point-bending test arrangement. In all tests the typical displacements and the bolt force distribution were measured. The end-plate plastic deformations were measured after the tests by an automatic measuring device. The measured data were presented and evaluated by the moment-bolt-row force and moment-distance from centre of compression diagrams and by the deformed end-plate surfaces. From the results the typical failure modes and the joint behaviour were specified and presented. Furthermore the influence of the end-plate thickness and the pretension of the bolts on the behaviour of bolted joints were analysed.

**Keywords:** bolted end-plate connection; beam-to-beam joint; experiment; four bolts in one bolt-row; HammerHead joint arrangement

---

### 1. Introduction

#### 1.1 Background

Steel industrial and agricultural halls as well as multi-storey steel buildings are widely designed to involve beam-to-column and beam-to-beam joints with bolted end-plates. Bolted solutions are easier to install and therefore cheaper and faster to build than their welded counterparts.

Until recent years, design of bolted joints, due to their complex behaviour and the wide variety of possible configurations – bolt number and arrangement, end-plate thickness, joint arrangement, stiffness, etc. –, has only been possible through conservative approaches. Current design standards,

---

\*Corresponding author, Ph.D., Assistant Professor, E-mail: [katula.levente@epito.bme.hu](mailto:katula.levente@epito.bme.hu)

including the Eurocode, offer more accurate calculation models that consider the effect of various components of the joint based on the rigidity and load-bearing capacity. An advantage of such models is that in most cases, they are able to reflect the consequences of modification in the joint arrangement during the design process, and give the flexibility to the designer to choose the final layout which suits the relevant internal forces as well as the applicable geometrical constraints.

The needs of the industry, however, tend to go beyond typical arrangements covered by design standards. In some cases, if the designer wishes to justify his joint concept, he will have to re-design it to achieve an arrangement preferred by the standard. This approach may, in the worst case, require a modification of the structural dimensions. An alternative is to calculate the ultimate load of standardised arrangements, and apply such arrangements up to certain levels of internal forces and moments. The disadvantage of this latter approach is that such standardised arrangements are fixed and no modifications are possible.

## 1.2 Previous studies

### Experimental studies

Until the end of the 1980s the following fields were in the focus of the experimental research of end-plate type joints: load-bearing capacity studies on different joints and bolt arrangements, cyclic behaviour studies, basic research on T-stubs. Tests were carried out and theories were developed worldwide (Piazza and Turrini 1989, Lacher 1987, Thiele and Reuschel 1989, Aribert *et al.* 1989, Nethercot *et al.* 1988).

In the 1990's the semi-rigid joint concept was substantially analyzed. Numerous tests were carried out to determine the joint behaviour under monotonic and cyclic loading (Bjorhovde *et al.* 1990, Zandonini *et al.* 1996, Jaspart 1997, Ádány *et al.* 2001).

### Analytical studies

End-plate connection design has been the subject of numerous studies since the early 1960's. Douty and McGuire presented in 1965 a method to determine the load bearing capacity of bolted end-plates that took the prying force effect into consideration. As this procedure was too complicated for practical use, the aim of the next research was to develop a simple model to determine the load-bearing capacity of end-plate connections. Significant progress was made in this field by Agerskov (1976), Mann and Morris (1979) and Grundy *et al.* (1980). A sophisticated approach to this problem was presented by Zoetemeijer (1974).

The principles of the component method are based on Zoetemeijer's work. Later, other researchers enhanced this method by determination the mechanical properties of further components and refinement of the calculation methods (Bjorhovde *et al.* 1990, Tschemmernegg 1992, Jaspart and Maquoi 1989, Piluso *et al.* 2008, Grecea *et al.* 2011). This improved the accuracy of the description of mechanical behaviour.

The accuracy of the component method depends on the accuracy of the description of the basic components and on the quality of the assembly process. It is assumed that the properties of the individual components are independent from each other. However, some components do not act independently but influence each other. For "hand calculation" this can be accounted for in a simplified way only, because the general approach results in a complicated iterative calculation procedure.

Since the 1990's finite element (FE) analysis has become a more and more important tool in joint research (Girao Coelho and Bijlard 2010, Shi *et al.* 2008).

### 1.3 Purpose of the study

The global aim of the research was to study the joint behaviour of different, non-conventional bolted, end-plate joint arrangements in order to develop design methods compatible with the Eurocode 3 based on the standardized component method model. The developed methods are to be verified and their accuracy is to be checked against the results of the tests completed.

The tested joint arrangements are used in portal frames of Lindab-Astron industrial buildings, and because of the innovative arrangements, there are uncertainties in their behaviour which are not supported by standardized design rule. The joint arrangements with four bolts in one bolt-row and HammerHead arrangement are studied experimentally to observe their behaviour.

EN 1993-1-8 (2005) describes detailed design rules for the calculation of bolted end-plate connections but with limitation in bolt arrangement. The method allows only two bolts in each bolt-row, which means one bolt on each side of the web plate. In certain cases it is more economical to apply four bolts in one row, which solution is commonly used and standardized e.g., in Germany, Sedlacek *et al.* (2001). However the Eurocode 3 analytical model can be developed and modified to connections with four bolts in one row – Demonceau *et al.* (2011), Sedlacek (2000). The goal of the authors was to develop an easy to use analytical model for this problem, which was verified by real size test results. Another innovative joint solution is the HammerHead arrangement that is not covered by the Eurocode 3.

The main aim of the experimental part of the research was to determine the failure mode and the joint behaviour for these types of joints in the light of the structural details and parameters.

The investigated joint types are summarized in Table 1. The end-plate arrangement (a) shows a standard joint that can be designed according to Eurocode 3; while the other arrangements raise design questions. The HammerHead arrangement, type (c), includes an extended end-plate part with two bolt-rows that is not covered by the standard. Arrangements (b), (d) and (e) show end-plates with four bolts in one row. Without standardized yield line patterns the resistances of T-stubs in these cases is rather ambiguous.

### 1.4 Research strategy

In the global research strategy interacting experimental, analytical and numerical tools were used. Experiments and derived results have a fundamental role and are the basis of the design method. Therefore, as a first step, an experimental programme was designed and completed. The experimental program included six different end-plate and bolt arrangements and covered sixteen specimens. Experiments were performed at the Structural Laboratory of the Budapest University of Technology and Economics. The accuracy of the developed Eurocode 3 compatible design method – for the four bolts in one row type end-plate joints and for HammerHead arrangements – was verified on the basis of the test results.

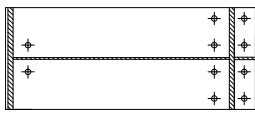
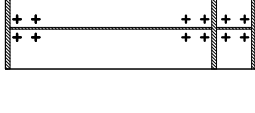
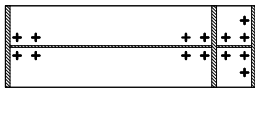
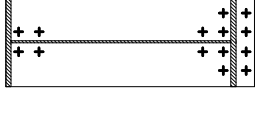
This paper has a focus on the experimental part of the research. The whole research study is presented in details in Katula (2007).

## 2. Research programme

### 2.1 Test specimens

The tested arrangements are presented in Table 1; these cover standard joint arrangements

Table 1 Test specimens

		test series B					
		Test series A					
end-plate arrangement							(a) Standard joint arrangement
		(b) Joint with four bolts in one row and additional stiffener in the first bolt-row	(c) HammerHead joint arrangement	(d) HammerHead joint arrangement and joint with four bolts in one row	(e) Joint with four bolts in one row		
	Joint type	I	II	III	IV	V	VI
	Design problem	-	The design problem indicated in (e) and additional stiffener in the first bolt-row.	In the extended tension zone the end-plate has two bolt-rows and an additional flange.	The design problems in (c) and (e) are combined in this arrangement.	In the end-plate the bolt-rows contain four bolts in the first and second row.	-
	Test specimen	TA TB	TE TF	TB2 TB6 TB10	TB3 TB7 TB11	TB4 TB8 TB12	TB5 TB9 TB13
	End-plate thickness $t_{ep}$ [mm]	16 20	20 24	12 15 20	12 15 20	12 15 20	12 15 20
Bolt grade (M20)		10.9			8.8		

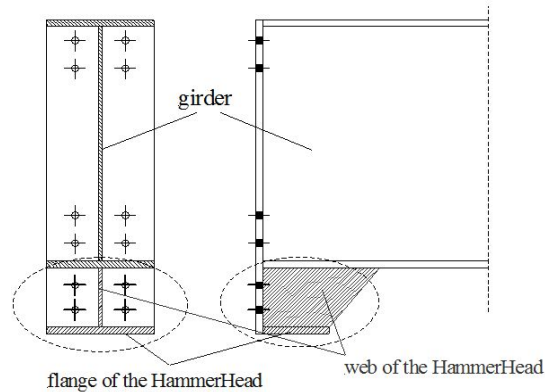


Fig. 1 HammerHead arrangement

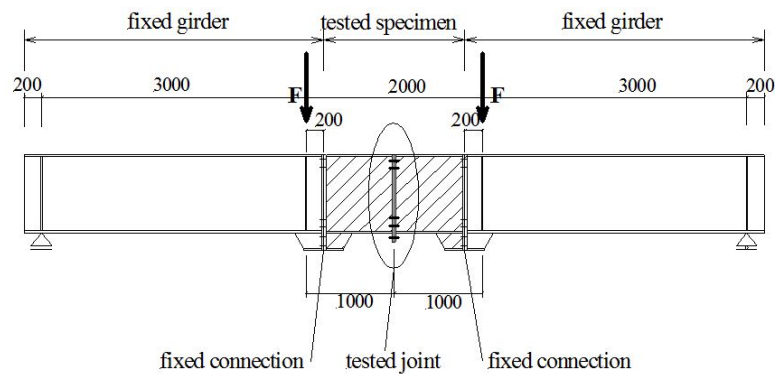


Fig. 2 Test arrangement

(end-plate types I and VI), joints with extended end-plates (types II, V and VI), as well as joints with four bolts in one bolt row (types II, IV and V), and the HammerHead arrangements (types III and IV). The HammerHead arrangement means an additional short web and flange, which are extended on the tension side of the girder as shown in Fig. 1.

## 2.2 Test arrangement

Beam-to-beam joints were investigated under pure bending conditions, applying a four-point-bending arrangement. The test setup used specimens connected to fixed girders by bolted end plates. This facilitated the replacement of specimens and provided the same boundary conditions for all tests. The specimens were erected between fixed girders, as shown in Fig. 2. Two concentrated loads were applied by hydraulic jacks with capacities of 400 kN.

## 2.3 Measuring system

### Displacements and bolt forces

During the tests representative displacements were measured by inductive transducers placed

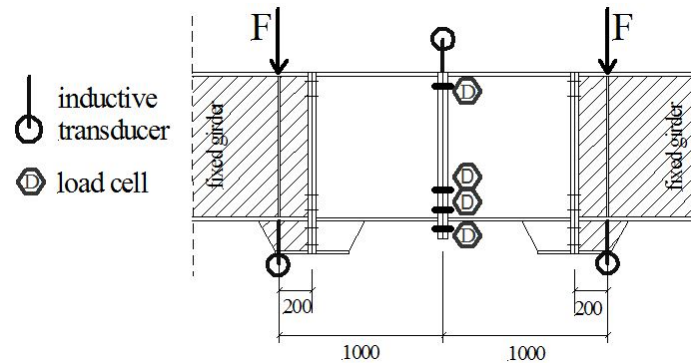


Fig. 3 Locations of transducers and load cells

under load introduction points and in the cross-section of the investigated joint. Distribution of bolt forces was registered by load cells, custom designed for this purpose. Measured data were collected at one second intervals by two HBM Spider data collection systems.

Fig. 3 shows schematically the locations of the transducers and the load cell.

#### End-plate deformations

Plate deformations were measured both in the elastic and in the plastic phase of the tests.

During the tests, in the elastic phase of joint behaviour, the end-plate deformations were measured by a portable inductive transducer – of the type Mitutoyo with a measuring range of 0.01 mm to 25 mm and an accuracy of 0.01 mm – and these collected data were evaluated after the tests.

Locations of the measuring points are presented in Fig. 4(a). The measuring points – drilled holes in the plate – were placed so as to give representative data on the expected deformation but at the same time not to disturb the development of yield lines or the load capacity of the joint. Therefore, on the one hand, an appropriate number of measuring points needed to be defined to

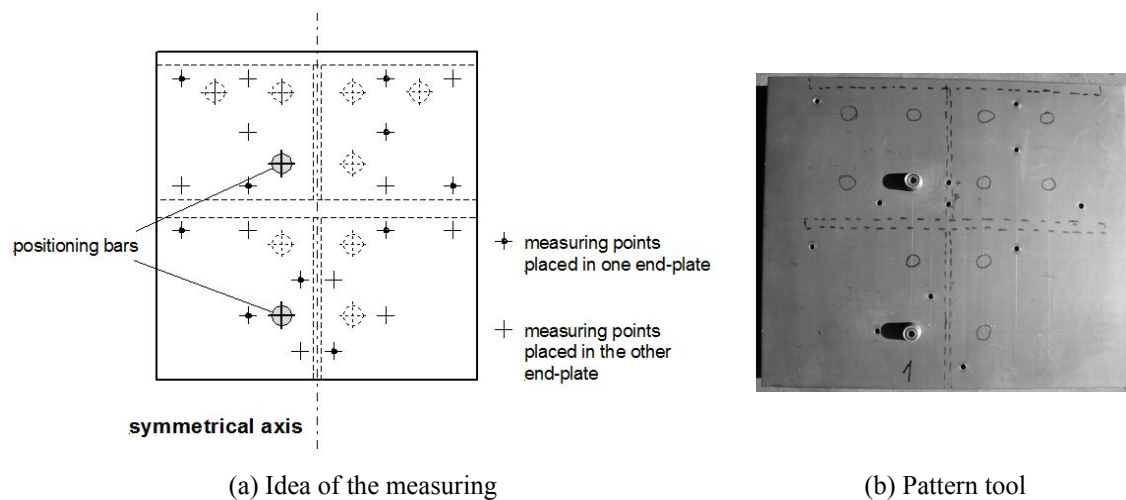


Fig. 4 Measuring method of plate deformations in the elastic phase



Fig. 5 Measuring the plastic deformations of the end-plate (specimen TB8)

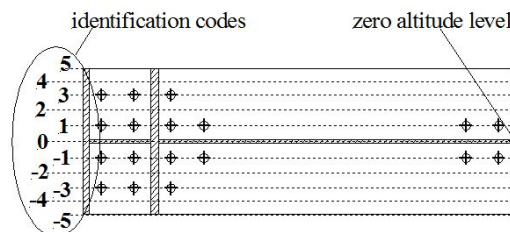


Fig. 6 Measured lines and identification codes

achieve an adequate accuracy of the deformation values determined, while on the other hand, one needed to be careful not to place too many points and disturb the yield line pattern development. For this reason half of the measuring points were placed in one end-plate, and the other half in the other plate, following a pattern symmetrical to the web.

Fig. 4(b) shows the fabricated pattern tool, which contained the holes marked bold only, and which was then applied in both end-plates making use of the symmetry of the bolt arrangement with respect to the web. For the exact positioning of the tool to the end-plates two positioning bars were used, as shown in Fig. 4(b).

After the test the plastic end-plate deformations were measured by an automatically running and measuring device, as shown in Fig. 5.

Benchmark data were collected in the web direction at each 0.25 mm, with the accuracy of 0.001 mm in terms of altitude. The zero altitude level was chosen for all end-plates at the intersection of the web and the compression flange, as shown in Fig. 6.

On each end-plate at least nine contour-lines were designated; Fig. 6 shows the layout of the measured contour-lines and the identification codes.

### 3. Test results

#### 3.1 Pretension force of the bolts

The bolts were preloaded in each test. The M20 bolts – and the M24 bolts in the fixed connection

– were pretensioned by a maximum pretension load of 200 Nm – and 450 Nm, respectively.

In order to get a homogeneous pretension force level in the joints a three-step preload process was used. First the bolts were strained by hand, then, beginning with the bolt-row farthest from the compression flange the bolts were preloaded by a pneumatic screwdriver, and in the third step – because of the end-plate deformations and other imperfections – the bolts were preloaded again with the pneumatic screwdriver.

Although the process described above was applied, the observed and measured pretension forces were inhomogeneous. This might be the result of the following effects:

- friction differences of the bolts (imperfect form, different coating thickness of the bolts),
- the bolt nut and/or bolt head was not exactly perpendicular to the end-plate (erection imperfection),
- inhomogeneous stiffness distribution between the bolt-rows in the end-plate (i.e. the connected plate parts adjacent to the flange had higher stiffness than the parts near the edge).

Table 2 summarizes the recorded pretension forces for each measured bolt and Fig. 7 shows the positions of the load cells.

Table 2 Measured pretension forces in the bolts in test series A and B

Bolt position	Name of the specimen pretension forces in kN															
	Test series A				Test series B											
	TA	TB	TE	TF	TB2	TB6	TB10	TB3	TB7	TB11	TB4	TB8	TB12	TB5	TB9	TB13
A	-	-	116.5	107.1	48.3	30.1	38.9	60.6	40.5	46.1	-	-	-	-	-	-
AA	-	-	114.2	106.4	-	-	-	67.1	78.9	43.2	-	-	-	-	-	-
A2	-	-	90.4	87.9	43.3	51.1	29.9	47.9	53.2	43.0	-	-	-	-	-	-
AA2	-	-	75.8	98.4	-	-	-	64.6	36.5	36.9	-	-	-	-	-	-
B	42.1	36.7	90.2	88.0	35.7	34.3	37.8	65.0	94.1	50.0	27.9	49.7	20.8	20.9	9.7	37.4
BB	-	-	97.7	85.6	-	-	-	-	-	-	36.9	28.5	18.4	-	-	-
B2	53.7	39.8	101.1	109.3	36.8	56.6	18.0	40.4	36.9	33.7	33.0	15.3	7.7	26.4	20.6	5.2
BB2	-	-	90.6	97.6	-	-	-	-	-	-	31.9	35.2	20.4	-	-	-
C	54.2	33.2	-	-	35.6	38.2	38.4	59.2	59.8	36.9	28.5	23.1	30.7	32.5	31.5	44.5
CC	-	-	-	-	-	-	-	-	-	-	36.2	29.2	59.2	-	-	-
C2	67.3	51.0	-	-	44.6	51.2	15.3	67.8	51.2	74.4	42.5	33.2	23.2	34.4	37.0	11.2
CC2	-	-	-	-	-	-	-	-	-	-	37.6	58.3	24.8	-	-	-
D	66.1	66.1	121.4	99.7	45.2	32.9	21.0	58.2	48.9	77.9	34.8	31.5	33.1	38.0	43.1	32.5
D2	85.5	85.5	124.4	115.4	41.5	59.6	28.6	52.4	68.3	49.2	34.8	47.0	43.7	31.3	27.2	29.4
E	-	-	-	-	49.1	58.0	26.9	44.2	47.4	62.6	39.5	39.4	37.0	-	58.4	39.8
E2	-	-	-	-	50.9	62.0	40.9	-	-	-	40.1	61.1	51.7	-	35.7	23.6
F	-	-	-	-	27.8	40.6	34.8	-	-	-	-	-	-	-	48.8	33.1
F2	-	-	-	-	35.4	54.4	49.3	-	-	-	-	-	-	-	34.1	11.2
	TA	TB	TE	TF	TB2	TB6	TB10	TB3	TB7	TB11	TB4	TB8	TB12	TB5	TB9	TB13

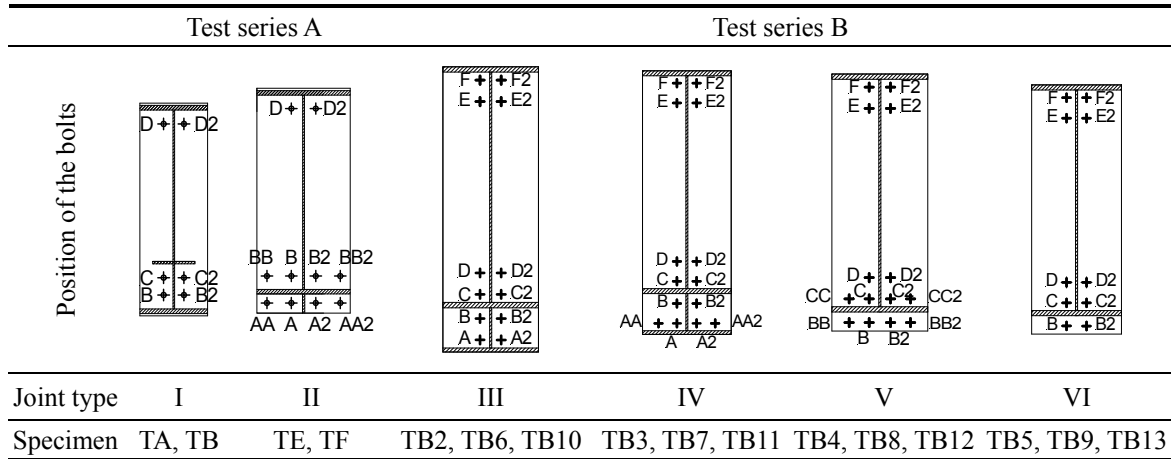


Fig. 7 Positions of the load cells

### 3.2 Test results

The data – collected during the tests – are prepared and presented by the moment vs. bolt-row force diagrams and figures of the deformed end-plate surfaces.

Because of different pretension levels of the bolts and different plastic deformations from previous load steps, the presented bolt-force curves have different starting points. Each diagram of the measured bolt forces presents the force of the whole bolt-row for clarity.

The moment vs. bolt-row force diagrams show how the force increment changes in the bolt-rows and which part of the joint – i.e., which bolt-row – resists higher forces.

The observed failure modes are discussed according to the definitions of Eurocode 3. Fig. 8 shows the possible T-stub failure modes: in Mode 1 the failure occurs in the form of plate yielding only, whereas Mode 2 is a combination of bolt failure and plate yielding. In both cases prying force will develop because of the closing of the edges of the plates; if the plate is thick enough, bolt failure develops (Mode 3).

#### Joint type I, standard joint arrangement

In Fig. 9 the diagrams show the result of test specimen TA ( $t_{ep} = 16$  mm). The moment vs.

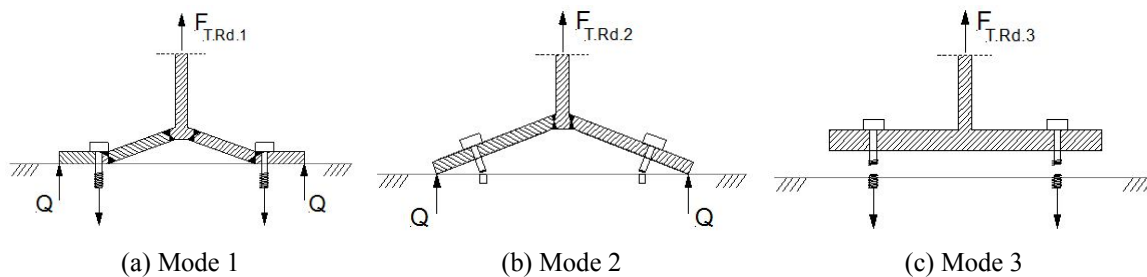


Fig. 8 T-stub failure modes according to Eurocode 3

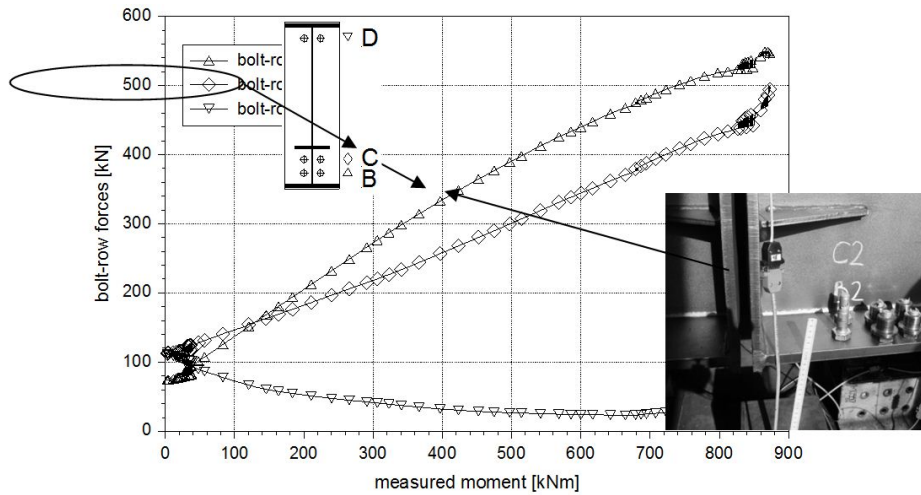


Fig. 9 Moment vs. bolt-row force diagrams of specimen TA

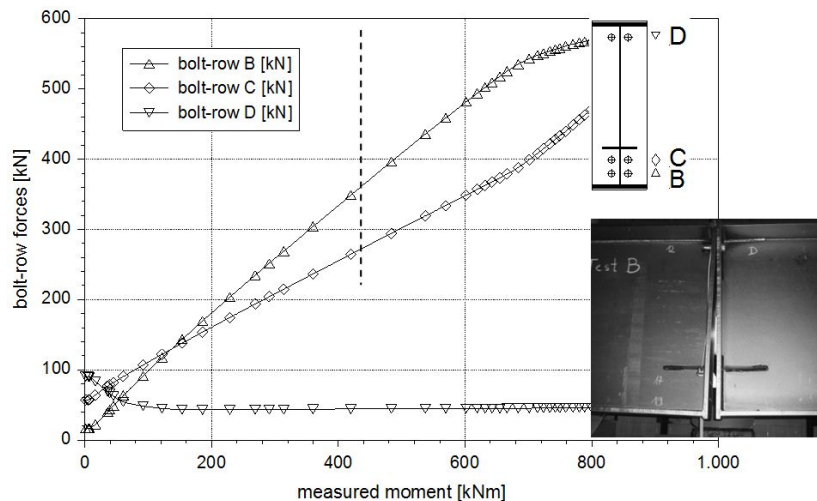


Fig. 10 Moment vs. bolt-row force diagrams of specimen TB

bolt-row force diagrams show the relationship of the measured force in the bolt-rows and the moment in the tested joint. The highest bolt-force increment was observed in bolt-row B, followed by bolt-row C. In case of failure Mode 1 well-defined changing cannot be observed in the moment vs. bolt-row force diagrams. During the loading process – before the load-bearing capacity is reached – the bolt forces increase proportionally to the external load. The prying effect is not visible on the curves. This can be explained by the stiffness relation between the thin end-plate and the high stiffness (10.9) M20 bolts.

Fig. 10 shows the diagrams of test specimen TB ( $t_{ep} = 20$  mm). Under the 700 kNm load level the bolt-row force distribution was similar to that of test TA. After that load level the diagrams become different. These breaking points show the end of the prying effect for bolt-row B and the

introduction of the prying effect for bolt-row C. Because of bolt elongations in the bolts in row B the plate edges do not contact any longer and the prying effect ceases to exist. This results in the reduced slope of curve B and the increased slope of the curve of bolt-row C.

For joint type I the calculated group failure in bolt-rows B and C was in the form of mixed bolt and plate failure (Mode 2). The experimental observation confirmed the results of the calculation for specimen TB. In case of specimen TA the calculation predicted mixed bolt and plate failure (Mode 2) instead of the observed plate failure (Mode 1).

#### Joint type II, joint with four bolts in one row and additional stiffener in the first bolt-row

Fig. 11 shows the bolt-row force diagrams for test specimen TE ( $t_{ep} = 20$  mm). The curve of bolt-row B shows a slight change in slope in the vicinity of the 1,400 kNm load level. This can be explained by plate deformations. After evolving plastic deformations in the joint, the edges of the end-plates close and the prying effect appears. The direct consequence of this effect is the increased slope of the diagram. This higher slope is the same as the slope of the curve A, which indicates that the bolt-rows up to this load level sustain the same deformations.

Results of test specimen TF ( $t_{ep} = 24$  mm) are presented in Fig. 12. The diagrams are similar to the results of test TE. An important difference is the lack of inflexion point on the results of bolt-row B that can be explained by the thicker end-plate in this specimen.

The developed analytical model predicted “horizontal” bolt group failure in Mode 2 in bolt-row A and bolt failure in bolt-row B for the specimen of joint type II. The observed failure mode confirmed the calculation; the ultimate behaviour of the joint was mixed bolt-and-plate failure (Mode 2) in bolt-row A and bolt failure in bolt-row B.

The developed analytical model and its evaluation are presented in details in Katula (2007).

#### Joint type III, HammerHead joint arrangement

Fig. 13 shows the moment vs. bolt-row force diagram of test specimen TB2 ( $t_{ep} = 12$  mm). The diagrams show that the highest force increment was measured in bolt-row C, followed by bolt-rows B, A and D. These results suggest that the bolt-force increments adjacent to the tension flange were the highest. A consequence of its large thickness ( $t_f = 20$  mm) (compared to the thin HammerHead flange and web) is the significant stiffness concentration near the tension flange.

Curve A shows a breaking point at the 1,150 kNm load level, which can be explained with the termination of the prying effect. Curves B, C and D show inflexion points at the 1,000 kNm load level. While the force increment in bolt-rows B and C decreases, in row D it is increasing.

Fig. 14 presents the result of specimen TB6 ( $t_{ep} = 15$  mm). The diagrams show similarities in bolt force behaviour for test specimen TB2. The highest force increment is in the bolt-rows adjacent to the tension flange. Bolt-rows B and C have two inflexion points. The first is around 300 kNm and the second around 1,100 kNm load level. After the first breaking point as a consequence of the evolving prying effect the curves slope increases. Above 1,100 kNm load level the rate of force increase in bolt-rows B and C decreases, whereas in rows D and slightly in row A further increase can be observed. This behaviour can be traced back to the termination and evolution of the prying effect, respectively.

Fig. 15 show diagrams for test specimen TB10 ( $t_{ep} = 20$  mm). The diagrams are similar to the results of test TB6. Because of the thicker end-plate the curves of bolt-row B and C show one breaking point only. This breaking point is at approximately the same load level (1,100 kNm). As an additional consequence of the thicker end-plate the prying effect for bolt-rows A and D are more visible.

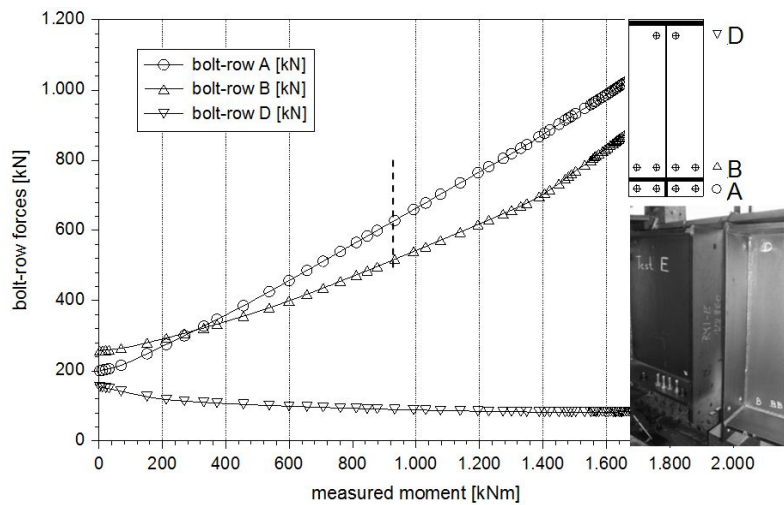


Fig. 11 Moment vs. bolt-row force diagrams of specimen TE

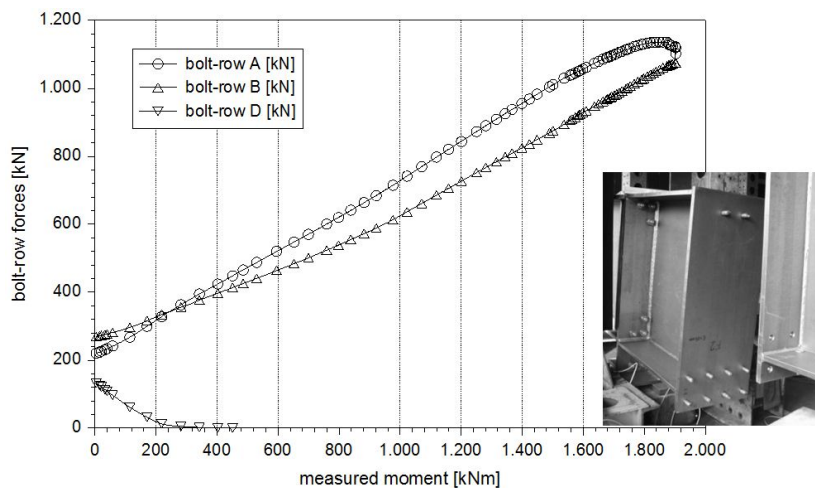


Fig. 12 Moment vs. bolt-row force diagrams of specimen TF

The calculated failure was bolt-group failure in the HammerHead part and group failure involving bolt-rows C and D between the flanges. The failure mode was Mode 2 for all groups except the test specimen TB2 ( $t_{ep} = 12$  mm) where Mode 1 was predicted in the HammerHead part. The observed failure confirmed calculation results but in case of specimen TB2 specified Mode 1 for bolt-rows C and D.

#### Joint type IV, HammerHead joint arrangement and joint with four bolts in one row

Fig. 17 presents the moment vs. bolt-row force diagrams of specimen TB3. The diagrams show that the bolt-force increments are higher in bolt-rows adjacent to the tension flange – in rows B and C – than in the other tension bolt-rows. This can be explained by the stiffness distribution in

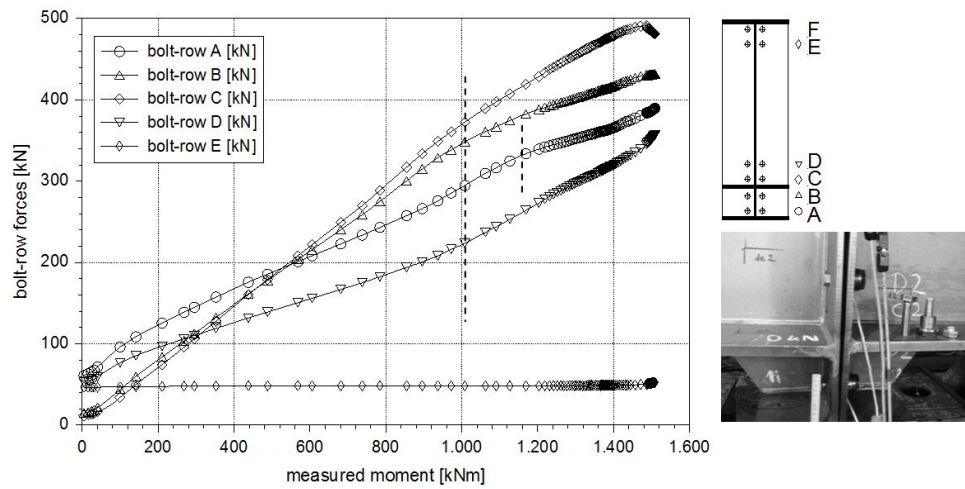


Fig. 13 Moment vs. bolt-row force diagrams of specimen TB2

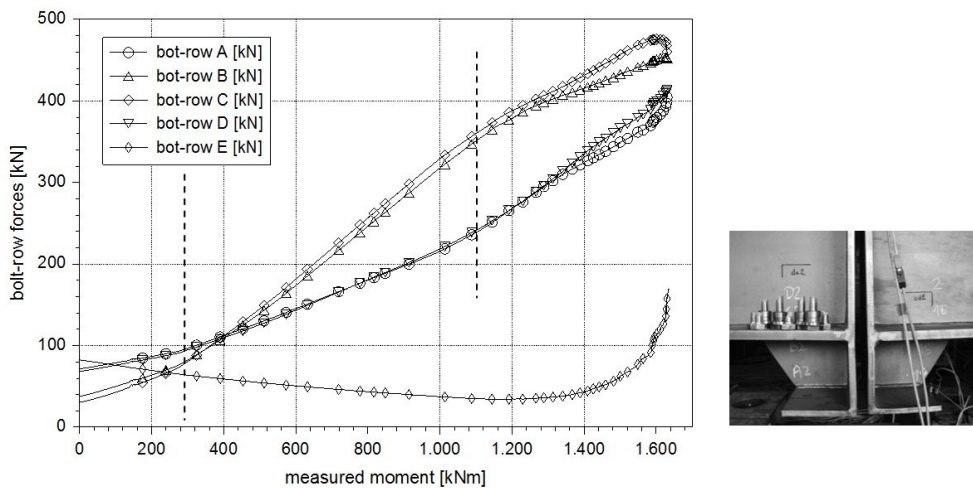


Fig. 14 Moment vs. bolt-row force diagrams of specimen TB6

the joint.

Curve A shows three breaking points, the first is at 500 kNm, the second at 1,100 kNm and the third at 1,400 kNm load level. The slope of the curve under the first and between the second and third breaking point is the same. The higher slopes between the first and second and above the third breaking point are also approximately identical. This indicates that the prying effect appeared at approximately 500 kNm, stopped at about 1,100 kNm and evolved from 1,300 kNm load level. The second appearance of the prying effect can be explained by the inhomogeneous stiffness distribution along the end-plate. Fig. 17 shows large end-plate deformations at the height of the girder's tension flange. This indicates that the short flange and web plate – as explained in Fig. 1 – in comparison to the girder's stiffness provide insufficient support of the end-plate in the HammerHead part. So the four bolts in bolt-row A can bend the end-plate at right angles to the

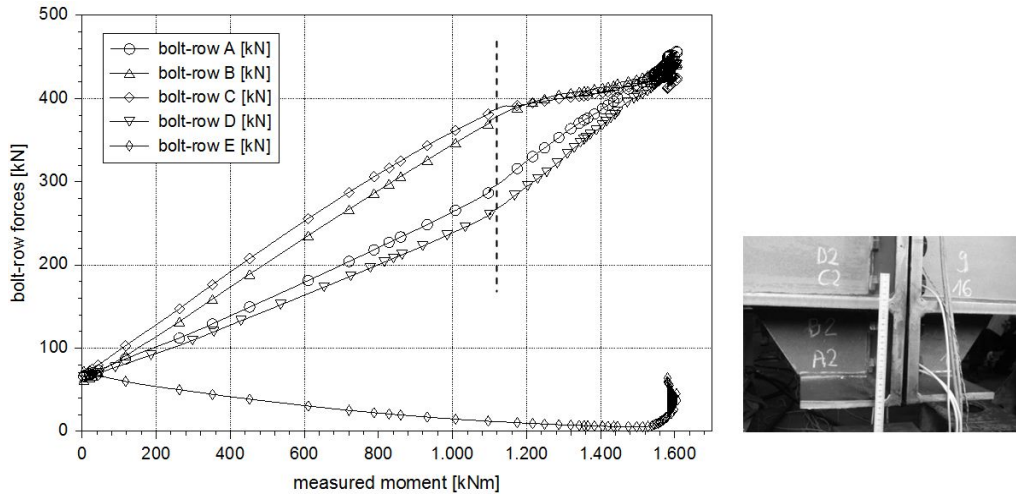


Fig. 15 Moment vs. bolt-row force diagrams of specimen TB10

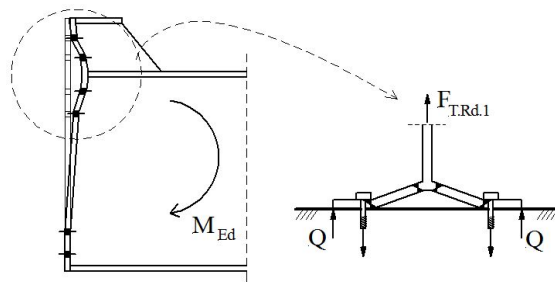


Fig. 16 End-plate deformations by HammerHead arrangement

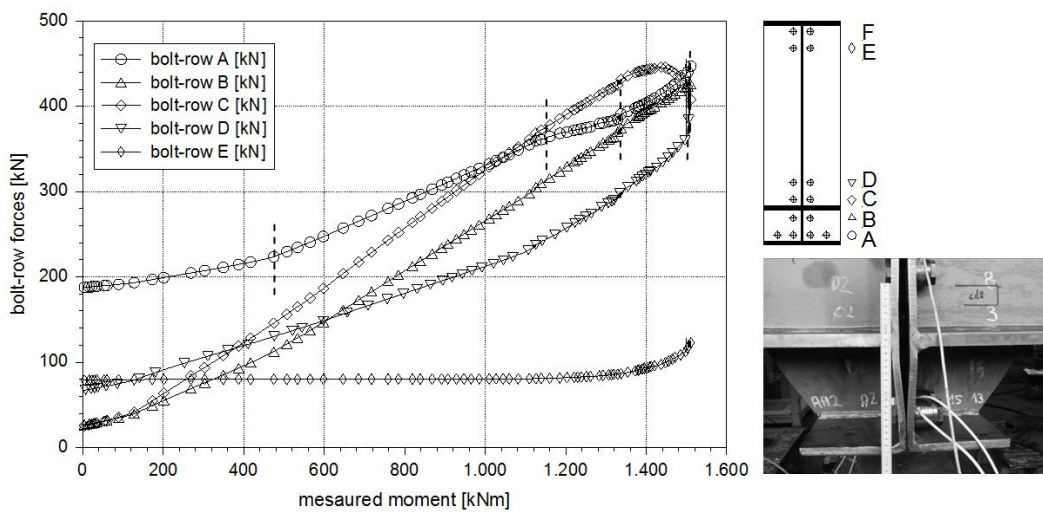


Fig. 17 Moment vs. bolt-row force diagrams of specimen TB3

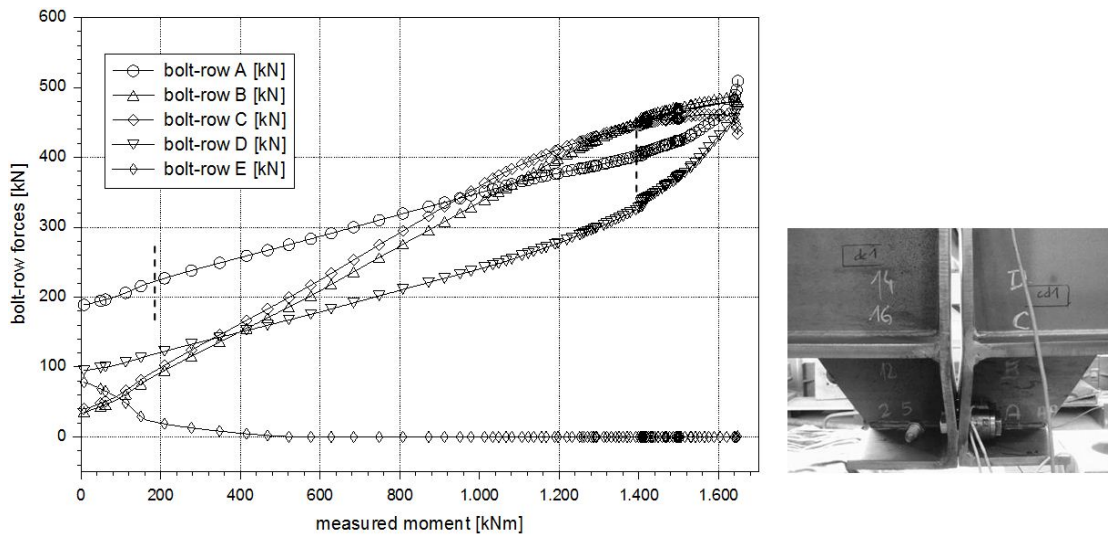


Fig. 18 Moment vs. bolt-row force diagrams, test TB7

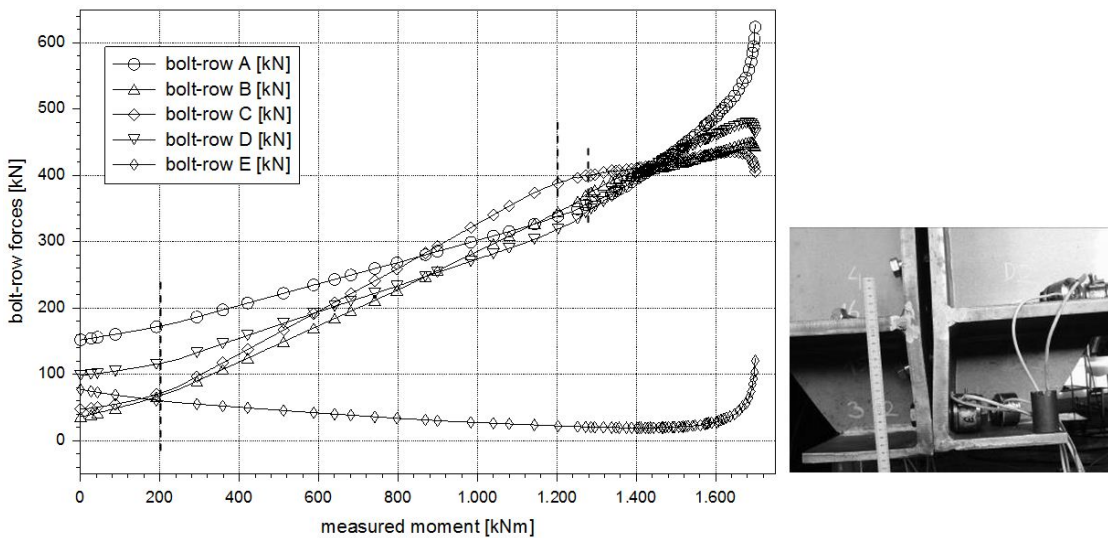


Fig. 19 Moment vs. bolt-row force diagrams, test TB11

web plate – see Fig. 16 for illustration. Curve D shows a slight change at the vicinity of 1.100 kNm load level, which stems from the evolving prying effect.

Fig. 18 shows the results of test specimen TB7 ( $t_{ep} = 15 \text{ mm}$ ). The observed behaviour of specimen TB7 is similar to that of specimen TB3. Curve A shows two breaking points, the first is at 200 kNm and the second at 1,400 kNm load level. The slope of the curve under the first and above the second breaking point is the same. This behaviour can also be explained by the prying effect. Because of the higher end-plate thickness compared to the test TB3, here no pure plate behaviour occurs in bolt-row A (i.e. curve A starts with the higher slope).

At approximately 1.300 kNm load level curves B, C and D show breaking points. The force increment in bolt-rows B and C decreases, while in row D it increases. The explanation of the change in trend lines is the same as in test TB3.

Fig. 19 shows the braking points more clearly than Figs. 17-18. The diagram of bolt-row A of specimen TB11 ( $t_{ep} = 20$  mm) shows a breaking point around the 1,400 kNm load level. After this load level the slope of the curve increases. This increase is explained by the “perpendicular” prying effect. Namely the bolts in bolt-row A bend the end-plate at right angles to the web plate similarly to tests TB3 and TB7. The diagram of bolt-row B shows clear breaking points at about 200 kNm and at the 1,300 kNm load level. The same tendency can be observed on the diagram of bolt-row C at the 200 kNm and at approximately 1,200 kNm load level. These changes in slope indicate the modification of the prying effect.

For specimen TB3 the calculated failure mode was group failure in the HammerHead part in Mode 1 and bolt-group failure involving bolt-rows C and D in Mode 2, which was confirmed with the test results. For specimens TB7 and TB11 bolt failure (Mode 3) was predicted in the HammerHead part and group failure in bolt-rows C and D in Mode 2. Because the calculation method uses a simple three-flange girder assumption for the HammerHead arrangements, it does not take into account any stiffness difference between the girder and the HammerHead part. Consequently, no angle deformation of the end-plate at the height of the tension flange was assumed. The observed failure was mixed plate and bolt failure in the HammerHead part and mixed plate and bolt failure in bolt-rows C and D as well.

#### Joint type V, joint with four bolts in one row

The observed failure mode for joint type V was similar to joint type IV. For all end-plate thicknesses the bolts bent the extended part of the end-plate as shown in Figs. 20-22.

The bolt-row force diagrams of test specimen TB4 ( $t_{ep} = 12$  mm) in Fig. 20 show only slight change in behaviour. On the diagram of bolt-row B one breaking point can be observed around 100 kNm load level. The final yield line pattern evolves up to this load level. Whereas the slope of

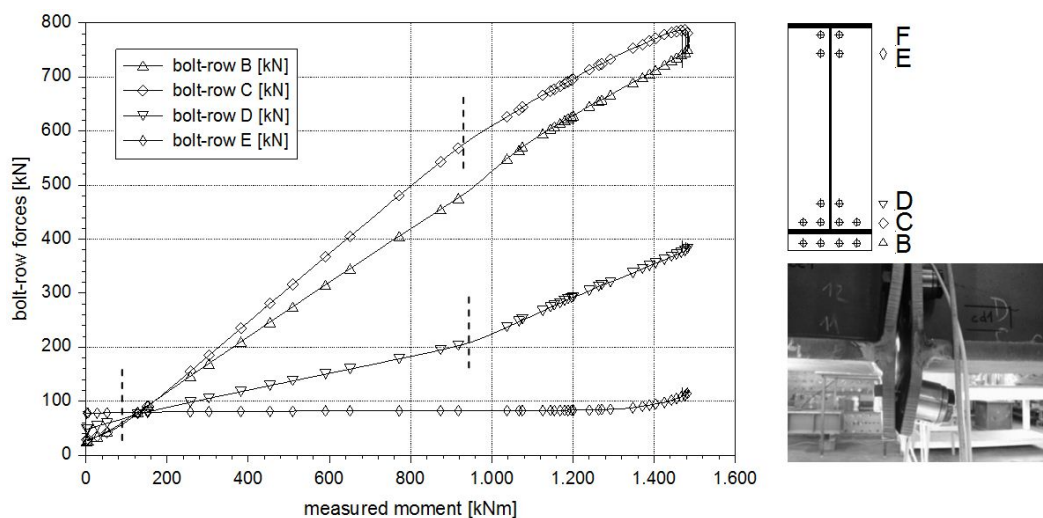


Fig. 20 Moment vs. bolt-row force diagrams, test TB4

the curve of bolt-row C changes slightly at two points, the first is at 100 kNm, the second at 900 kNm load level. The curve of bolt-row D has two breaks at about 150 kNm and at 900 kNm load levels. Contrary to the observation of other trend lines, curve D has a higher starting slope, which decreases from 150 kNm and increases again after 900 kNm load level. This phenomenon can be explained by the stiffness relationship between plate and bolt and the bolt arrangement. Because of bolt elongations on higher load levels, the prying effect vanishes. But after significant plate and bolt deformations the “perpendicular” prying effect is introduced and the slope of the diagram increases again.

In the calculation of bolt-row B – bolts in the extended part – group failure was predicted and

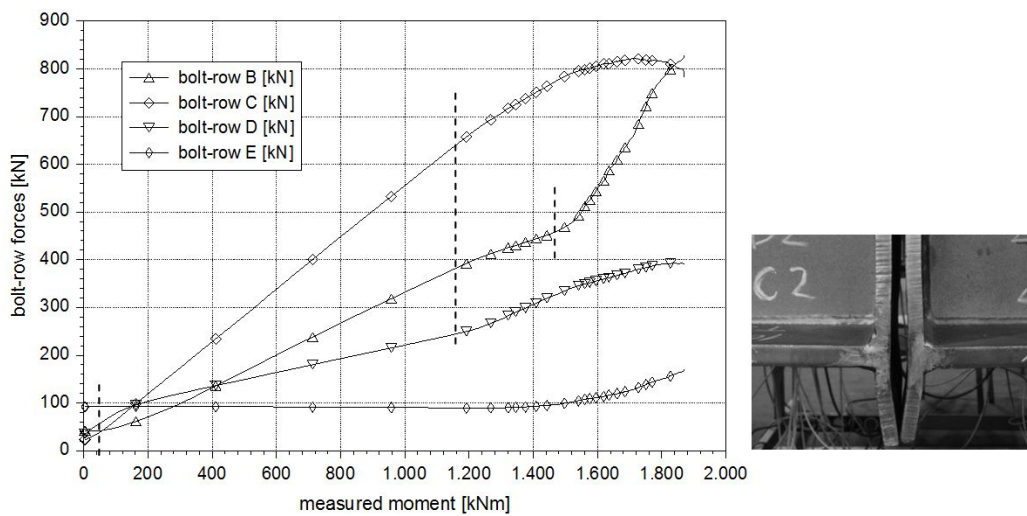


Fig. 21 Moment vs. bolt-row force diagrams, test TB8

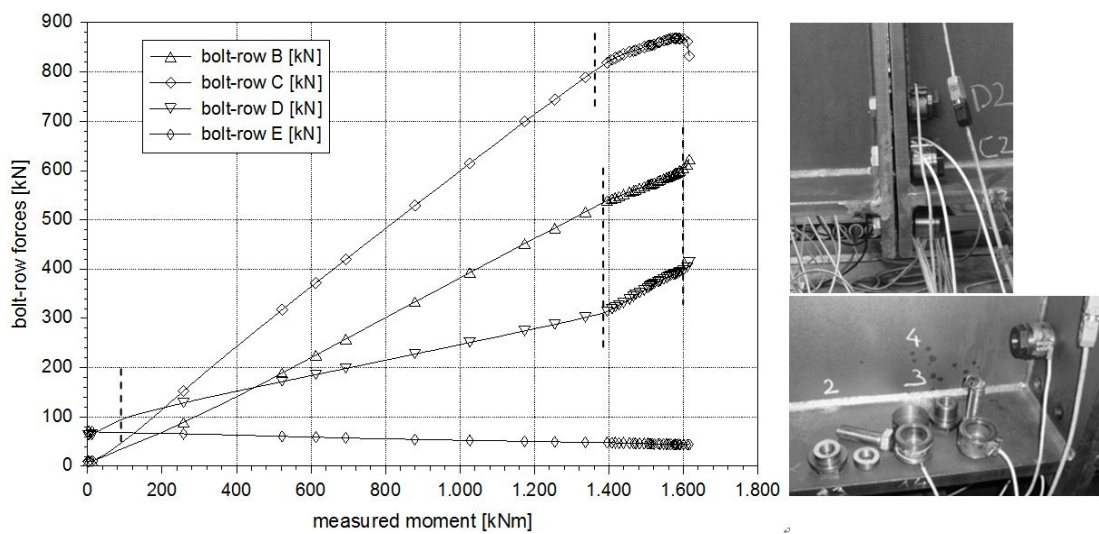


Fig. 22 Moment vs. bolt-row force diagrams, test TB12

group failure in bolt-rows C and D was expected as well. The measured data confirmed the results of the calculation. The ultimate behaviour of the joint was governed by plate failure.

Fig. 21 shows the results of test specimen TB8 ( $t_{ep} = 15$  mm). The diagram of bolt-row B shows three breakpoints. The first is at 100 kNm, the second at 1,200 kNm and the third at 1,500 kNm load level. The third breakpoint shows that after the upper end-plate edges closed the “perpendicular” prying effect evolved. The curve of bolt-row C shows two breakpoints similarly to the specimen TB4 but at higher load levels. The first is at approximately 100 kNm, the second at 1,200 kNm load level. These changes in behaviour follow the plate deformations, i.e., the evolution and vanish of the prying effect. Curve D shows similarities with the observation of specimen TB4. Consequently, curve D has a higher starting slope, which decreases and increases afterwards. The trend curve of bolt-row D exhibits changes at the load levels about 150 kNm and 1,200 kNm.

Fig. 22 presents the diagrams of test specimen TB12 ( $t_{ep} = 20$  mm). The thicker end-plate shifts the breakpoints to higher load levels. The diagram of bolt-row B shows three breakpoints similarly to Fig. 21. The first is at 100 kNm, the second at 1,400 kNm and the third at 1,600 kNm load level. Because of the height of the applied load cells, the bolts were not long enough and their threaded part sawed only 3 or 4 threads within the cells. This caused premature failure in the threads of the bolts and reduced their load bearing capacity. The diagram of bolt-row C shows two breakpoints similarly to specimens TB4 and TB8. The first is at approximately 100 kNm, the second at 1,400 kNm load level. The explanation for these changes in behaviour is the same as for specimen TB8. The trend lines for bolt-row D present similarities in all tests for joint type V. The first breakpoint is at approximately 100 kNm in every test. The higher the end plate thickness, the higher the second breakpoint is on the diagram.

For joint type V the calculated failure mode in bolt-row B was “horizontal” bolt group failure in Mode 1, which was confirmed by the results. For bolt-rows C and D the calculated failure in case of TB4 was group failure in Mode 2, and in cases TB8 and TB12 was Mode 3. Test results showed group failure in Mode 2 in all cases for joint type V between the flanges.

#### Joint type VI, standard joint arrangement with extended end-plate

Fig. 23 shows the bolt-row force diagrams of test specimen TB5 ( $t_{ep} = 12$  mm). The diagram of bolt-row B shows the same phenomenon like bolt-row D in joint type V. Namely the initial slope of the curve is higher than the slope after the first breakpoint. This phenomenon is explained by the stiffness relationship between the end-plate and bolt and the bolt arrangement. The prying effect can be observed from the beginning of the loading. Curve B has two breakpoints. The first is at approximately 100 kNm, the second at 800 kNm load level. The trend line of bolt-row C also shows two breakpoints; the first is at about 100 kNm, the second at 800 kNm load level. These points indicate the change in the prying effect.

Results of the specimen TB9 ( $t_{ep} = 15$  mm) are displayed in Fig. 24. On the curve of bolt-row B one breakpoint is shown at the 100 kNm load level. The curve of bolt-row C shows two breakpoints similarly to test specimen TB5. The load levels and explanation of the behaviour is similar to test TB5. Trend line D shows similar shape as curve B of specimen TB5. The curve has two breakpoints and the initial slope of the curve is higher than the slope after the first breakpoint. Fig. 25 shows the bolt-row force diagrams of test specimen TB13 ( $t_{ep} = 20$  mm). A consequence of the thick end-plate is the constant slope of the curve of bolt-row B. The curve of bolt-row C shows slight change around the 800 kNm load level. Trend line D shows similarities to curve D of specimen TB9, however, because of the thicker plate here only one breakpoint appears at

800 kNm.

The calculated failure mode for joint type VI was “horizontal” bolt group failure in the extended bolt-row in Mode 1 for specimen TB5 and in Mode 2 for specimens TB9 and TB13. Between the flanges group failure – involving bolt-rows C and D – in Mode 2 was predicted. The measured deformations and observed failure confirm the results of the calculation.

### 3.3 Load-bearing capacities

Table 3 summarizes the measured load-bearing capacities of tested joints. For test series B the same beam geometry was used and only the joint arrangements were different. The last row of Table 3 shows the proportion of the measured moment resistance of the joint and the moment

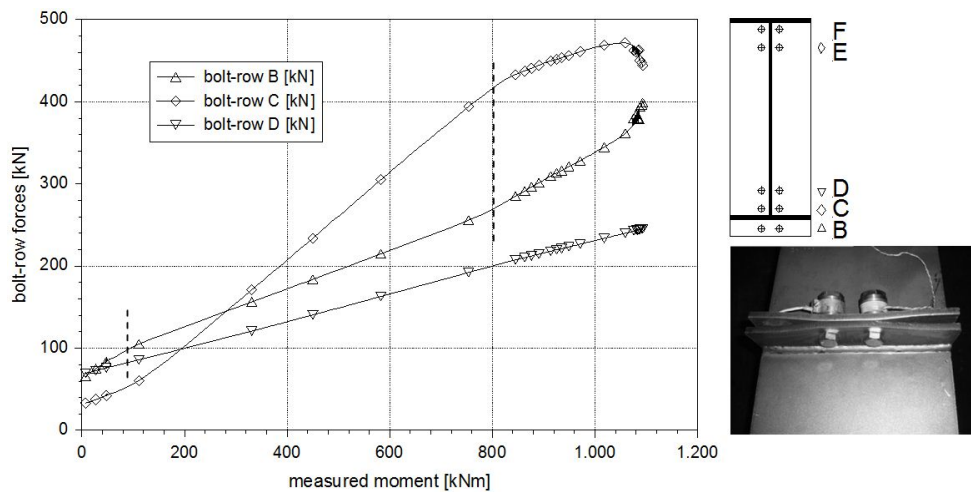


Fig. 23 Moment vs. bolt-row force diagrams, test TB5

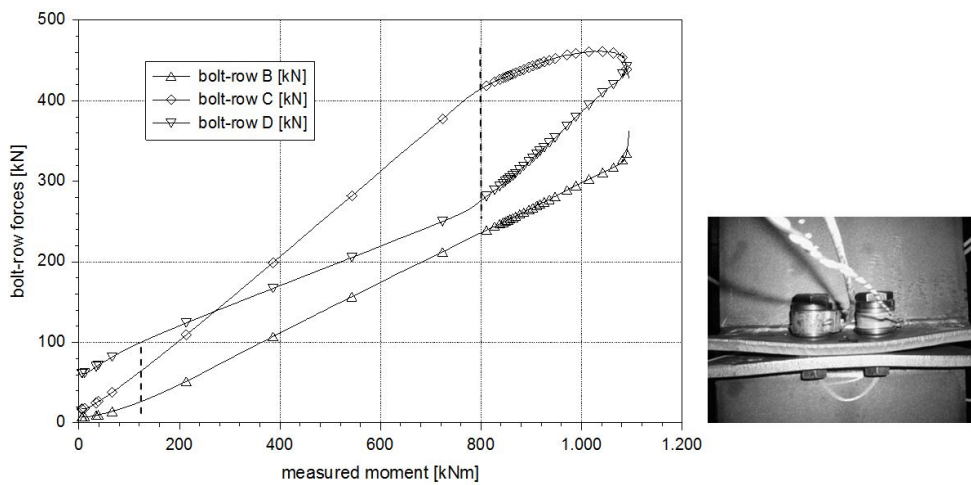


Fig. 24 Moment vs. bolt-row force diagrams, test TB9

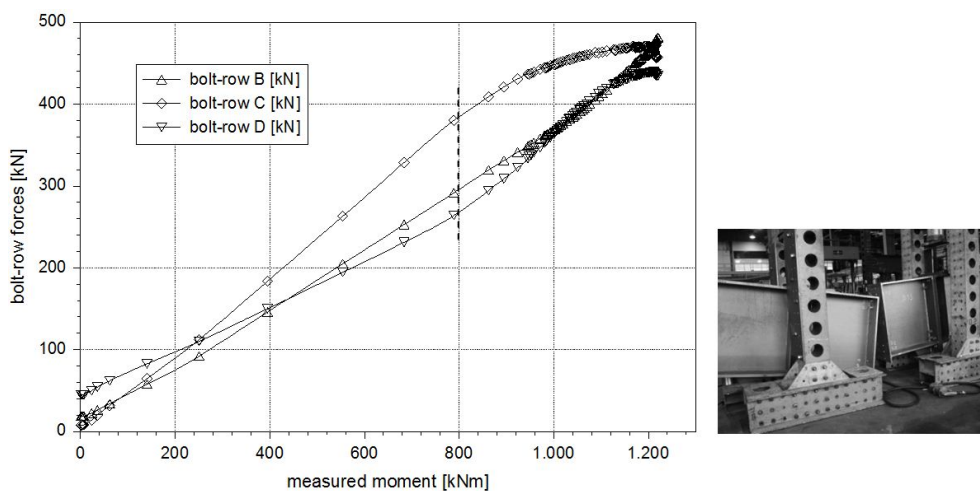


Fig. 25 Moment vs. bolt-row force diagrams, test TB13

Table 3 Experimental load-bearing capacities

	Test series A						Test series B												
End-plate arrangement																			
Joint type	I	II	III	IV	V	VI	I	II	III	IV	V	VI	I	II	III	IV	V	VI	
Test specimen	TA	TB	TE	TF	TB2	TB6	TB10	TB3	TB7	TB11	TB4	TB8	TB12	TB5	TB9	TB13			
End-plate thickness $t_{ep}$ [mm]	16	20	20	24	12	15	20	12	15	20	12	15	20	12	15	20			
Ultimate load [kN]	291	300	626	634	503	545	536	504	550	567	495	623	539	370	365	407			
$M_j/M_{beam}^1$ [%]	36	37	57	58	64	69	68	64	70	72	63	79	68	47	46	52			

<sup>1</sup> moment resistance of the joint / moment resistance of the beam

resistance of the beam. The specimens with thicker end-plates achieved higher capacities. The only exception is end-plate type V where the specimen TB8 ( $t_{ep} = 15$  mm) shows higher capacity than TB12 ( $t_{ep} = 20$  mm). In specimen TB12 the bolts failed in their threaded part, which caused a premature failure for the joint and explains the deviation from expected results.

The results presented in Table 3 show the positive effect of the HammerHead arrangement and the advantages to using four bolts in one row. Taking the results of end-plate type VI as a reference, with the load bearing capacity increases by 31-50% with the HammerHead arrangement (type III), 31-72% with four bolts in one row solution (type V) and 36-52% with a combined arrangement (type IV) 36-52%.

### 3.4 End-plate deformations

The objective of measuring end-plate deformations in the elastic phase was to analyse the load vs. deformation relationship in order to investigate how plate deformations develop up until the ultimate limit state.

In the EN 1993-1-8(2005) standard the design method to determine the end-plate deformations – i.e., the yield line pattern – in the ultimate limit state is specified, but it does not inform about the load-deformations equilibrium in the phases when the behaviour is still elastic. The goal was to identify the “path” that leads from elastic to plastic deformations and to find the relationship between these deformations.

The presented diagrams show relative deformations. The initial deformations due to the welding process and the erection were measured and taken into consideration as the reference surface for the purposes of further measurements.

The end-plate deformations in the calculated elastic phase were measured in the case of end-plate thicknesses 12 mm and 16 mm only, because here higher deformations were expected.

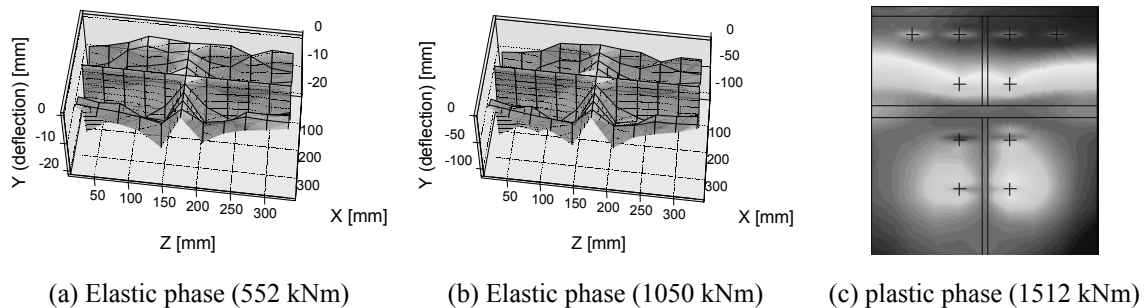


Fig. 26 The end-plate deformations in the elastic and the plastic phases of the specimen TB3

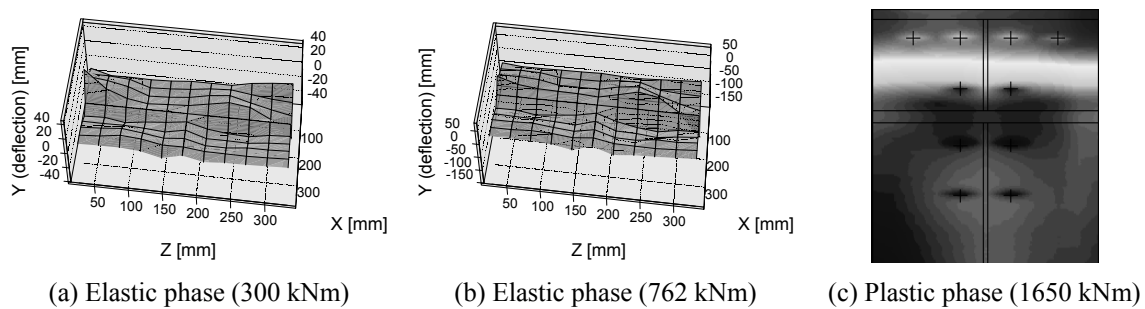
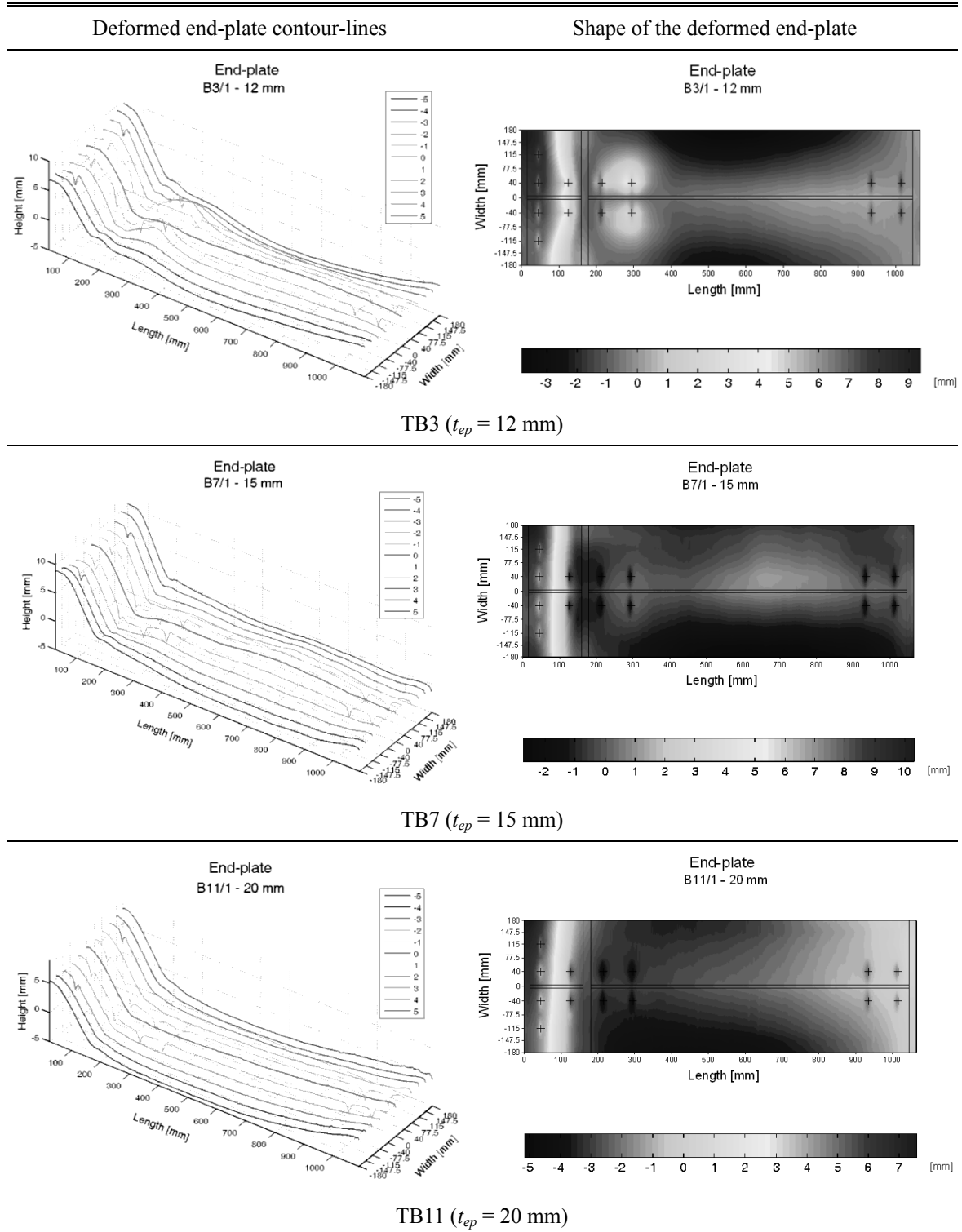


Fig. 27 The end-plate deformations in the elastic and the plastic phases of the specimen TB7

Table 4 End-plate deformation of specimens, joint type IV



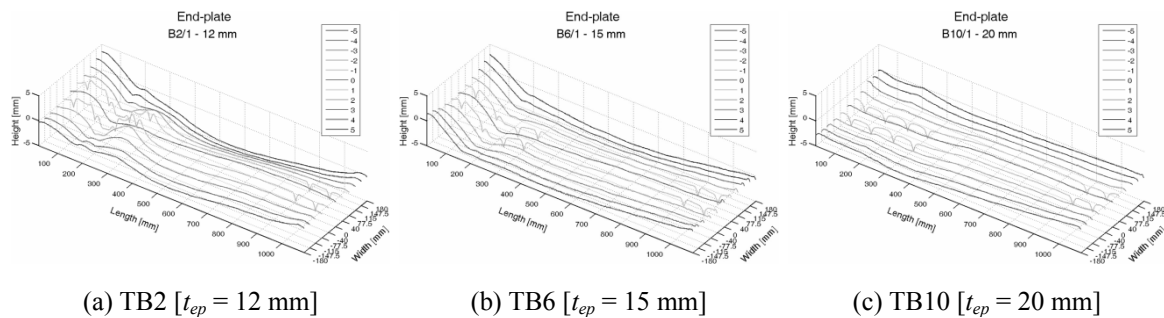


Fig. 28 Deformed end-plate contour-lines, joint type III

The surfaces presented below have been obtained by interpolation between the measured points. The deformed shapes were generated with the assumption that the plate cannot deform along the line of the web and of the flange.

Figs. 26(a) and (b) show the end-plate deformations of specimen TB3 in the elastic phase as an example, while the plastic deformations are displayed in Fig. 26(c). The deformed shape of the end-plate—as shown in Fig. 26(c)—was calculated by linear interpolation between the contour-lines.

The plate deformations of specimen TB7 are presented in the elastic phase in Figs. 27(a)-(b), while the plastic deformations are illustrated in Fig. 27(c).

From the measured results in the elastic phase it is concluded that the 3D deformation diagrams show similar deformations as those corresponding to the ultimate failure already at relatively low load levels that correspond to the elastic phase of joint behaviour. This shows that the governing end-plate deformations can already be identified in the elastic phase. The proposed end-plate measuring method in the elastic range can be applied for forecasting the end-plate type failure modes.

Table 4 summarizes the results of the measurements of the deformed end-plate of specimens TB3, TB7 and TB11 after the test. Deformations are presented by contour-lines in the left column and deformed surfaces are shown in the right column. The end-plate type IV joints show typical large deformations at the height of the HammerHead flange. The reason is the stiffness difference between the girder and the HammerHead part.

The deformations of the joint type III joints are shown in Fig. 28. Typical plate deformations at the height of the HammerHead flange can be observed on Figs. 28(a) and (b) only. These deformations are similar to those from end-plate type IV. But Fig. 28(c) shows a different behaviour without specific plate deformations which can stem from the higher end-plate thickness.

#### 4. Result evaluation

On the basis of the measured bolt forces and end-plate deformations, the change of position of the centre of compression and the effect of plate thickness on the failure mode was identified and it is presented in the form of moment–distance from centre of compression diagrams (see Fig. 29 for illustration).

According to EN 1993-1-8 (2005) the position of the centre of compression in ultimate limit state is defined as the centre of the stress block of the compression forces, i.e., the mid-point of the

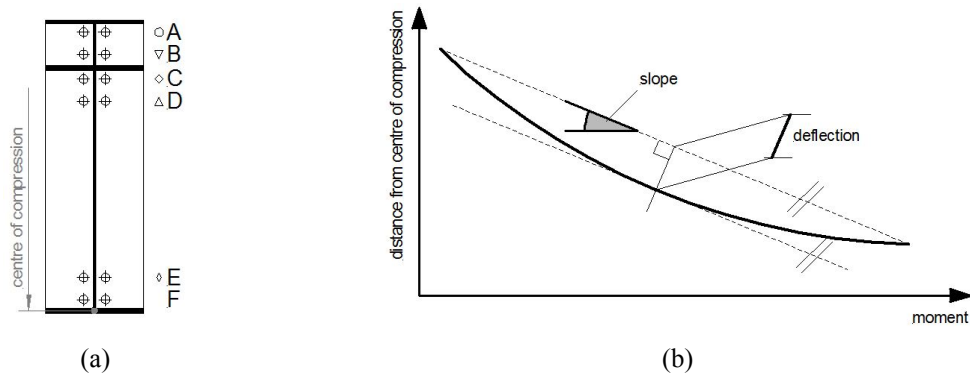


Fig. 29 The meaning of slope and deflection of the diagram

compression flange. It is obvious, however, that this position is a function of external loading. If the bolt forces are known, the change of position of the centre of compression can be calculated taking into account the equilibrium of moments within the joint.

Based on the test results the influence of the end-plate thickness on the position of the centre of compression of the joints was studied. In the trivial case where the end-plate has significantly higher stiffness than the applied bolts, the bolt forces are proportional to the distance from the centre of compression. In this case end-plate deformations are negligible and the load vs. centre of compression diagram is linear.

For the same joint arrangement the thinner the plate, the higher the slope of the load vs. centre of the compression diagram. The slope means the angle between the horizontal axis and the line, which is fitted on the end-point of the diagram, as shown in Fig. 29.

In the practically applied end-plates, however, the deformations are not negligible and these affect the position of the centre of the compression. In fact the pretension force level is a second parameter, which also influences the diagram. The evaluation of the results showed that for accurate results the homogeneous pretension force level is beneficial.

The “deflection” of the curve is an indicator of the pretension level. The higher the deflection of the diagram the lower the sum of pretension level.

The position of the actual centre of compression can be calculated from the moment equilibrium as given in Eq. (1)

$$F_{load} \cdot l = \sum F_{bolt,r} \cdot h_r \quad (1)$$

where  $F_{load}$  is the actual external load [kN];  
 $l$  is the lever arm of the load [m];  
 $F_{bolt,r}$  is the tension load in bolt-row  $r$  [kN];  
 $h_r$  is the distance from bolt-row  $r$  to the centre of compression [m];  
 $r$  is the bolt-row number.

Figs. 30 and 32 illustrate representative moment vs. distance from centre of compression relationships of joint types III and IV. The slopes of the curves show the influence of end-plate thickness. The higher the slope corresponds to thinner end-plates. Deflections indicate pretension levels. Figs. 31 and 33 show the moment vs. summarized bolt-row force diagrams, where the sum

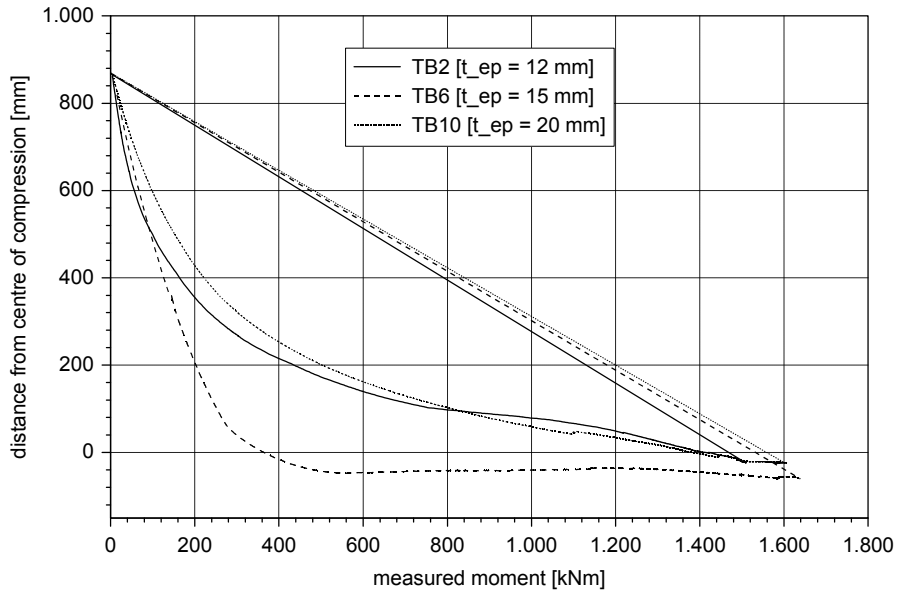


Fig. 30 Moment vs. distance from centre of compression diagrams of joint type III

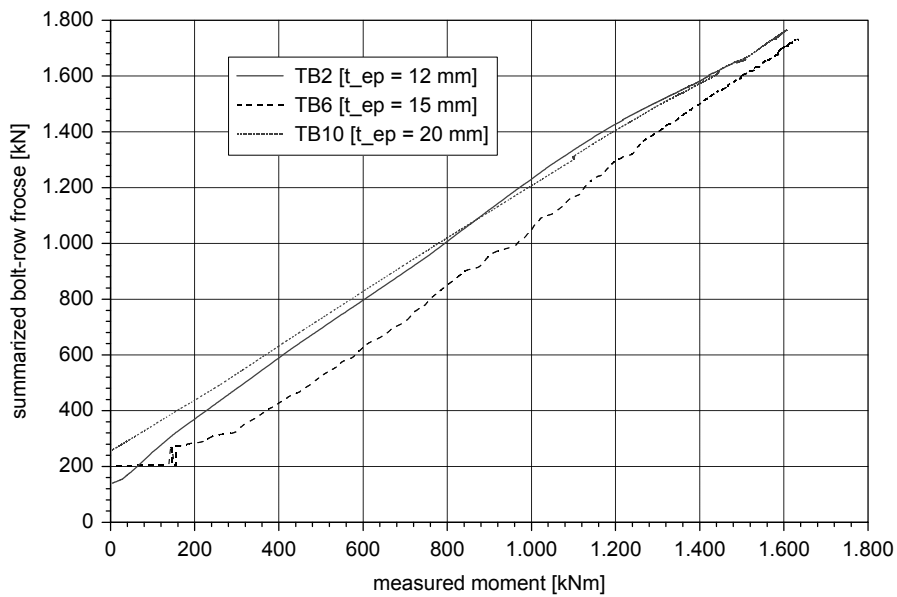


Fig. 31 Moment vs. summarized bolt-row forces diagrams of joint type III

of the bolt-row forces (A + B + C + D) of the tension zone are shown on the vertical axis. The diagrams highlight that the higher the sum of the bolt forces is the smaller the deflections become. A higher pretension level assures a smoother moment vs. distance from centre of compression diagram, i.e., a beneficial rotational behaviour.

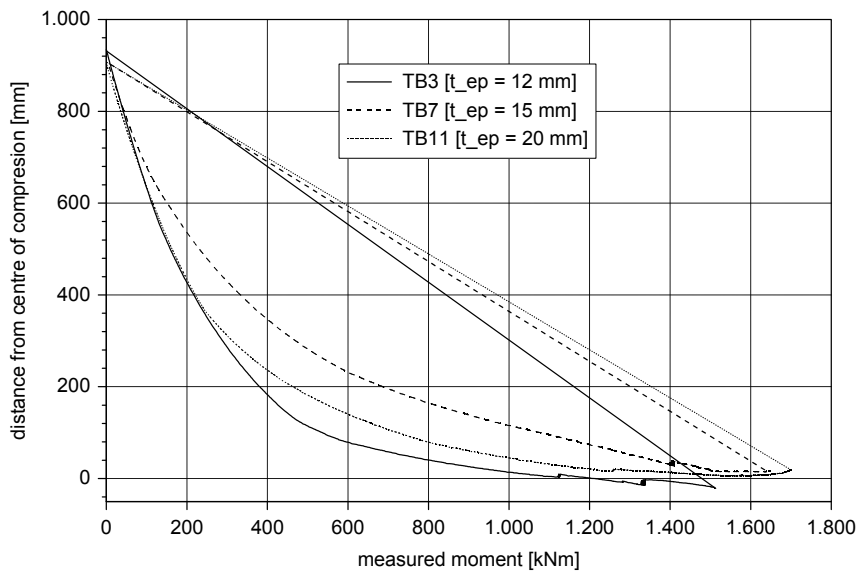


Fig. 32 Moment vs. distance from centre of compression diagrams of joint type IV

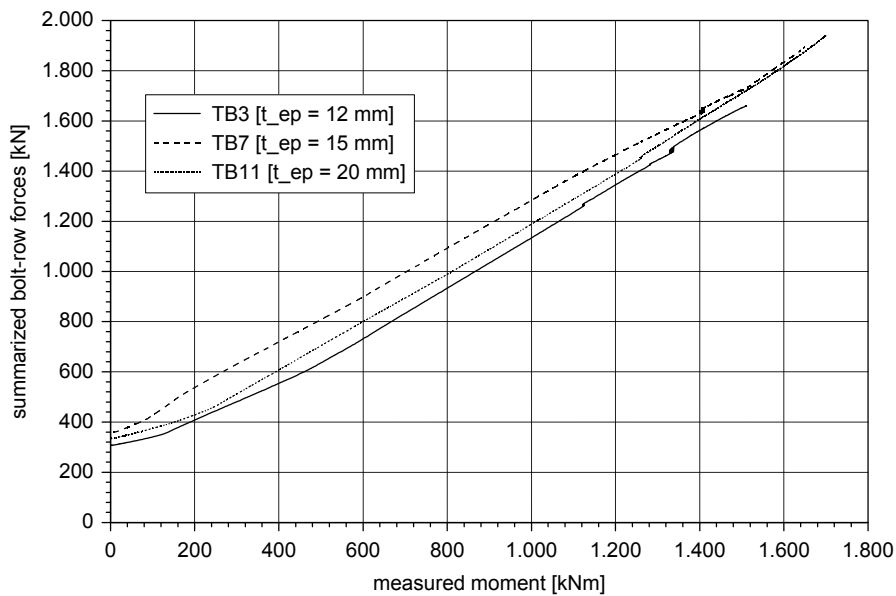


Fig. 33 Moment vs. summarized bolt-row forces diagrams of joint type IV

## 5. Conclusions

Experimental investigation of bolted beam-to-beam end-plate joints is presented in this paper. Standard and innovative – HammerHead arrangements and four bolts in one bolt-row – joint specimens were tested under pure bending conditions. From these results the typical failure modes

and the joint behaviour were specified and presented. Furthermore, the influence of the end-plate thickness and the effect of the pretension of the bolts on the behaviour of bolted joints were studied.

It is proven that the four bolts in one row joint arrangement (joint type II, IV, and V) is a competitive solution, enhances the load-bearing capacity effectively (up to 72%) without increasing the required end-plate height. This is especially beneficial when the overall end-plate dimensions are limited.

The efficiency of the solution can be increased by higher HammerHead arrangement. Experimental results show that up to 50% higher load-bearing capacity can be achieved with this solution. The combination of the two arrangements is also presented in the research.

On the basis of the measured bolt forces and end-plate deformations the paper points out that the stiffness distribution within the joint has significant influence on bolt forces; on this basis the optimal bolt arrangement can be designed.

The measured load vs. deformation relationship of the end-plate confirmed that the governing end-plate deformations can already be identified in the elastic phase. This fact can be used for forecasting the failure mode.

Based on the test results the influence of the plate thickness on the position of the centre of compression of the joints was studied. The evaluated results show that the thinner the end-plate the higher the slope of the load vs. centre of the compression diagram. The pretension level of the bolts influences the deflection of the curve. With higher pretension a beneficial rotational behaviour can be assured.

In relation to the tested HammerHead joints a “perpendicular” prying effect was detected which deforms the end-plate on both sides of the tension flange symmetrically. This phenomenon enhances the moment resistance of the joint similarly to the prying effect, but leads to plastic deformations at the same time.

## Acknowledgments

The experimental research work was completed by the financial support of Lindab-Astron; the authors wish to thank for their helpful collaboration. The first author is grateful for the support of the Bolyai Research Scholarship.

## References

- Ádány, S., Calado, L. and Dunai, L. (2001), “Experimental study on the cyclic behaviour of bolted end-plate joints”, *J. Steel Compos. Struct.*, **1**(1), 33-50.
- Agerskov, H. (1976), “High-strength bolted connections subject to prying”, *J. Struct. Div., ASCE*, **102**(1), 161-175.
- Aribert, J.M., Brozzetti, J. and Ryan, I. (1989), “Behaviour of bolted end plate connections of large dimensions”, *Proceedings of International Colloquium, Bolted and Special Structural Connections*, (Volume 2), Bolted Connections Subjected to Tension and Bending, USSR Moscow, Russia, May, pp. 39-46.
- Bjorhovde, R., Colson, A. and Brozzetti, J. (1990), “Classification system for beam-to-column connections”, *J. Struct. Eng.*, **116**(11), 3059-3076.
- Douty, R.T. and McGuire, W. (1965), “High strength bolted moment connections”, *J. Struct. Div., ASCE*, **91**(ST2), 101-128.

- EN 1993-1-8 (2005), Eurocode 3: Design of steel structures, Part 1-8: Design of Joints.
- Demonceau, J.-F., Jaspert, J.-P., Weynand, K., Oerder, R. and Müller, C. (2011), "Connections with four bolts per horizontal row; Application of Eurocode 3", *EUROSTEEL 2011*, Budapest, Hungary, September, Volume A, pp. 567-572.
- Girao Coelho, A.M. and Bijlard, F.S.K. (2010), "Finite element evaluation of the strength behaviour of high-strength steel column web in transverse compression", *J. Steel Compos. Struct.*, **10**(5), 385-414.
- Grecea, D., Dubina, D. and Muntean, N. (2011), "Beam-to-column joints of bolted extended end-plate; Influence of T-stub failure mode on the global performance", *EUROSTEEL 2011*, Budapest, Hungary, September, Volume A, pp. 201-206.
- Grundy, P., Thomas, I.R. and Bennetts, I.D. (1980), "Beam-to-column moment connections", *J. Struct. Div., ASCE*, **106**(1), 313-330.
- Jaspert, J.P. (1997), "Recent advances in the field of steel joints, Column bases and further configurations for beam-to-column joints and beam splices", Thesis; Université de Liège, Liège, Belgium.
- Jaspert, J.P. and Maquoi, H. (1989), "Simple design method for sway frames with semi-rigid connections", *Proceedings of International Colloquium, Bolted and Special Structural Connections*, (Volume 3), Bolted Connections Subjected to Tension and Bending, USSR Moscow, Russia, May, pp. 72-79.
- Katula, L. (2007), "Bolted end-plate joints for crane brackets and beam-to-beam connections", Ph.D. Dissertation; Budapest University of Technology and Economics, Budapest, Hungary.
- Lacher, G. (1987), "Dauerschwingversuche an axialbeanspruchten Schrauben 10.9 in T-Verbindungen", *Stahlbau*, **56**(9), 257-266.
- Mann, A.P. and Morris, L.J. (1979), "Limit design of extended end plate connections", *J. Struct. Div., ASCE*, **109**(3), 511-526.
- Nethercot, D.A., Davison, J.B. and Kirby, P.A. (1988), "Connection flexibility and beam design in non-sway frames", *Eng. J., AISC*, **25**(3), 99-108.
- Piazza, M. and Turrini, G. (1989), "The post-elastic behaviour of the end-plate connection with preloaded bolts", *Proceedings of International Colloquium, Bolted and Special Structural Connections*, (Volume 2), Bolted Connections Subjected to Tension and Bending, USSR Moscow, Russia, May, pp. 89-96.
- Piluso, V., Rizzano, G. and Sabatino, R. (2008), "Prediction of ultimate behaviour of bolted T-stubs: influence of bolt preloading", *EUROSTEEL 2008*, Graz, Austria, Volume A, pp. 513-518.
- Sedlacek, G. (2000), "Plastische Bemessung von Stirnplatten-Anschlüssen mit 4 Schrauben in einer Reihe", DASt Forschungsbericht 5/2000, RWTH Aachen.
- Sedlacek, G., Weynand, K. and Oerder, S. (2001), "Typisierte Anschlüsse im Stahlhochbau", (Band 1 und 2), Deutscher Stahlbau-Verband DSTV, Stahlbau-Verlagsgesellschaft GmbH. [In German]
- Shi, G., Shi, Y., Wang, Y. and Bradford, M.A. (2008), "Numerical simulation of steel pretensioned bolted end-plate connections of different types and details", *Eng. Struct.*, **30**(10), 2677-2686.
- Thiele, R. and Reuschel, E. (1989), "Experimental determination of the moment-rotation behaviour of not prestressed header plate joints", *Proceedings of International Colloquium, Bolted and Special Structural Connections*, (Volume 2), Bolted Connections Subjected to Tension and Bending, USSR Moscow, Russia, May, pp. 131-135.
- Tschemmerneegg, F. (1992), "The non-linear behaviour of composite joints", *J. Construct. Res.*, **21**, 59-70.
- Zandonini, R., Zanon, P. and Bernuzzi, C. (1996), "Experimental analysis and modelling of semi-rigid steel joints under cyclic reversal loading", *J. Construct. Steel Res.*, **38**(2), 95-123.
- Zoetemeijer, P. (1974), "A design method for the tension side of statically loaded bolted beam-to-column connections", *Heron*; Delft, The Netherlands, **20**(1), pp. 1-59.